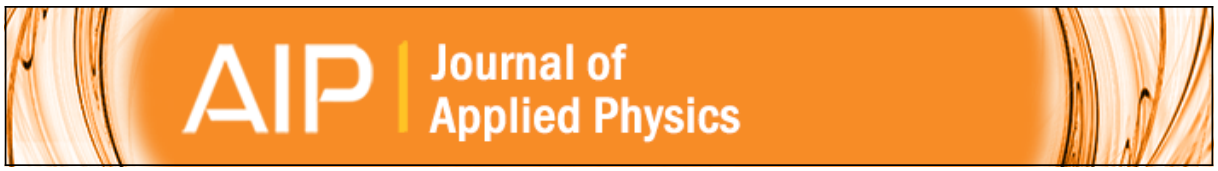

CdCl2 treatment related diffusion phenomena in Cd1xZnxS/CdTe solar cells

G. Kartopu, A. A. Taylor, A. J. Clayton, V. Barrioz, D. A. Lamb, and S. J. C. Irvine

Citation: Journal of Applied Physics **115**, 104505 (2014); doi: 10.1063/1.4868224
View online: http://dx.doi.org/10.1063/1.4868224
View Table of Contents: http://scitation.aip.org/content/aip/journal/jap/115/10?ver=pdfcov
Published by the AIP Publishing

$CdCl_2$ treatment related diffusion phenomena in $Cd_{1-x}Zn_xS$/CdTe solar cells

G. Kartopu,[1,a)] A. A. Taylor,[2] A. J. Clayton,[1] V. Barrioz,[1] D. A. Lamb,[1] and S. J. C. Irvine[1]
[1]*Centre for Solar Energy Research (CSER), Glyndŵr University, OpTIC, St. Asaph Business Park, St. Asaph LL17 0JD, United Kingdom*
[2]*Physics Department, Durham University, Durham DH1 3LE, United Kingdom*

(Received 1 August 2013; accepted 28 February 2014; published online 14 March 2014)

Utilisation of wide bandgap $Cd_{1-x}Zn_xS$ alloys as an alternative to the CdS window layer is an attractive route to enhance the performance of CdTe thin film solar cells. For successful implementation, however, it is vital to control the composition and properties of $Cd_{1-x}Zn_xS$ through device fabrication processes involving the relatively high-temperature CdTe deposition and $CdCl_2$ activation steps. In this study, cross-sectional scanning transmission electron microscopy and depth profiling methods were employed to investigate chemical and structural changes in CdTe/$Cd_{1-x}Zn_xS$/CdS superstrate device structures deposited on an ITO/boro-aluminosilicate substrate. Comparison of three devices in different states of completion—fully processed ($CdCl_2$ activated), annealed only (without $CdCl_2$ activation), and a control (without $CdCl_2$ activation or anneal)—revealed cation diffusion phenomena within the window layer, their effects closely coupled to the $CdCl_2$ treatment. As a result, the initial $Cd_{1-x}Zn_xS$/CdS bilayer structure was observed to unify into a single $Cd_{1-x}Zn_xS$ layer with an increased Cd/Zn atomic ratio; these changes defining the properties and performance of the $Cd_{1-x}Zn_xS$/CdTe device. © *2014 AIP Publishing LLC*. [http://dx.doi.org/10.1063/1.4868224]

I. INTRODUCTION

One of the current research themes on CdS/CdTe thin film devices focusses on finding a suitable alternative to CdS thinning in order to further improve device characteristics by boosting the device blue/ultraviolet response. The spectral response of a recent record CdTe device (18.3% best efficiency)[1] displayed uniform and high external quantum efficiency (EQE) values down to ~300 nm, which cannot be practically achieved by CdS thinning. Further, to prevent shunting pathways and low photovoltage regions, the application of ultrathin CdS (≤50 nm) necessitates the insertion of a high resistivity metal-oxide buffer layer between the transparent conducting oxide (TCO) and CdS. In these respects, utilisation of a thicker window layer based on wide bandgap Cd-based compounds, such as $Cd_{1-x}Zn_xS$ alloys[2] or nanocrystalline CdS:O,[3] is foreseen to change practices in the fabrication of CdTe photovoltaic devices. However, successful implementation of such window layers requires good understanding and control of the window layer properties through subsequent fabrication processes and within the final device structure.

The effects of $CdCl_2$ treatment in CdS/CdTe solar cells, regarding the structural and chemical changes within the bulk of the CdTe absorber and at the metallurgical interface, are extensively documented. In summary, the grains in CdTe usually enlarge and re-crystallise, and their p-type carrier concentration rises (for treatment in air/O_2 environment).[4–6] Meanwhile, crystal defect density due to the 10% lattice mismatch at the CdS/CdTe interface may be reduced through the formation of a CdS_xTe_{1-x} interlayer.[7–9] However, little attention has been paid to the possible changes taking place within the window layer and its interface to the TCO. Investigating these changes could be of paramount importance for CdTe devices utilising Cd-based ternary alloys as the window layer. A previous study on ultrathin $Cd_{1-x}Zn_xS$/CdTe devices suggested that Zn was leaching out from the window layer for very thin CdTe absorbers (≤500 nm), reducing the gain in blue-response.[10] Zn diffusion into the CdTe absorber was also reported by Zhou *et al.* in a $ZnSnO_x$/$Cd_{0.92}Zn_{0.08}S$ (50 nm)/CdTe cell structure.[11]

Performance of $Cd_{1-x}Zn_xS$/CdTe solar cells fabricated by atmospheric pressure metalorganic chemical vapour deposition (AP-MOCVD) has been studied as a function of Zn content and a nominal value of $x = 0.7$ was found to be optimum.[2] In this study, a detailed investigation is carried out on $Cd_{1-x}Zn_xS$/CdTe solar cells using transmission electron microscopy (TEM) and depth profiling methods to identify the structural and optical transformations occurring in the window layer as a result of post-deposition treatments ($CdCl_2$ activation and/or anneal).

II. EXPERIMENTAL DETAILS

Fabrication details of $Cd_{1-x}Zn_xS$/CdTe devices using AP-MOCVD have been provided in previous publications.[2,10] Briefly, an ITO/boro-aluminosilicate substrate was first coated with a 50 nm CdS seed layer, at the relatively low deposition temperature of 315 °C and growth rate of 0.2 nm/s, to aid the uniform nucleation of the $Cd_{1-x}Zn_xS$ ($x = 0.7$) window layer, which was deposited subsequently at 360 °C. The total thickness of the bi-layer structure was 240 nm. Then, CdTe was deposited at 390 °C using arsenic (As) as the p-type dopant. The As concentration was varied from 10^{18} atoms/cm^3 in the bulk (2000 nm) to $\geq 10^{19}$ atoms/cm^3 at the CdTe surface (250 nm),

a)Author to whom correspondence should be addressed. Electronic mail: giray.kartopu@glyndwr.ac.uk. Tel.: +44-1745-535-213.

i.e., the back contact layer (BCL), yielding a npp$^+$ structure[12] $CdCl_2$ activation was achieved by coating a layer of $CdCl_2$ onto the CdTe surface by MOCVD at 200 °C and then annealing at 420 °C for 10 min in a flowing H_2 environment. Three device states were investigated: as-deposited, annealed, and activated. The as-deposited device received no $CdCl_2$ coating or anneal, the annealed device had the post-growth anneal (10 min at 420 °C in H_2 ambient) without $CdCl_2$ deposition while the activated device received both.

Optical transitions taking place in the window layer were monitored by comparing the transmittance spectrum of $Cd_{1-x}Zn_xS$/CdS (450/50 nm) reference bi-layers deposited on boro-aluminosilicate glass with the EQE spectrum of $CdCl_2$ activated CdTe/$Cd_{1-x}Zn_xS$/CdS/ITO/boro-aluminosilicate device structures. Cross-sectional TEM coupled with energy-dispersive X-ray spectrometry (EDS) measurements were made on the samples to investigate compositional and structural changes. Additionally, depth profiling of key elements (Cd, Te, S, Zn, Cl, As, and O) was obtained using secondary ion mass spectroscopy (SIMS) on a Cameca ims 4f spectrometer (LSA Ltd., Loughborough) employing Cs^+ primary ions, in order to identify the composition of working ($CdCl_2$ activated) device structures. For these measurements, a 1×1 cm^2 specimen was cleaved from each device and etched in a diluted bromine/methanol solution to reduce surface roughness prior to measurements.

Detailed comparisons were made between as-deposited, $CdCl_2$ activated, and annealed device structures using TEM/EDS methods in order to understand the role(s) of post-deposition treatments in structural and optical changes, particularly regarding the window layer. These measurements were carried out in scanning mode (STEM) with a JEOL 2100F microscope. The EDS (Oxford INCAx-Sight) measurements were also performed in STEM-mode by acquiring spectra along lines and varying the distance from the ITO interface. The measurement of sulphur in CdTe was carried out as part of a larger study into sulphur diffusion[13] and a 1% sulphur in CdTe standard was available to make these measurements fully quantified. The TEM/EDS measurements of the $Cd_{1-x}Zn_xS$/CdS layers were performed without standards and therefore an accuracy of ±3 at. % is assumed. Additionally, energy filtered TEM (EFTEM) images were acquired in conventional TEM mode using a commercial energy filter (Gatan Tridiem). The STEM images were also acquired under high angle annular dark field (HAADF) conditions; this results in the contrast of the images being dependent on the average atomic number of the material being penetrated, assuming a constant material thickness. The samples analysed were prepared by the focussed ion beam lift-out technique.[14] Several precautions were taken in order to minimise the effects of ion beam damage and Ga-implantation. First, the electron beam was used to coat the area of interest with a 1 μm Pt protective layer prior to sample thinning. Second, the accelerating voltage of the ion beam was gradually reduced such that final polishes were carried out on both sides of the sample with only 2 kV and then 1 kV beam accelerations; this strongly limits the depth to which Ga is implanted into the final sample.

III. RESULTS AND DISCUSSION

A. Evidence of Zn diffusion and intermixing in the window layer

Figure 1(a) gives the transmittance spectra of $Cd_{1-x}Zn_xS$/CdS (450/50 nm) reference bi-layers, with x ranging from 0 (CdS) to 0.91. It is clear that while the optical gap of $Cd_{1-x}Zn_xS$ widens with increasing Zn content, the existence of the CdS seed layer is also indicated from the presence of filter-like absorption edges at ~500 nm, corresponding to the CdS bandgap of ~2.4 eV. Conversely, the EQE spectra of $CdCl_2$ activated CdTe devices employing the $Cd_{1-x}Zn_xS$/CdS window layer structure (with x up to 0.70) did not display the double-edge structure seen in the transmittance spectra of reference layers (Fig. 1(b)). Instead, a uniform, single-edge that is blue-shifted in line with increasing Zn content can be observed. From these data, it can be inferred that an intermixing occurs between the corresponding layers resulting in a single composition $Cd_{1-x}Zn_xS$ window layer.

In order to better visualise the devices and separate out the effects of $CdCl_2$ activation and the high-temperature processing, TEM measurements were performed on the as-deposited, annealed, and activated device structures employing a $Cd_{0.3}Zn_{0.7}S$/CdS window layer (Figs. 2 and 3). From the bright field (BFSTEM) micrographs, while both CdS and $Cd_{1-x}Zn_xS$ layers can be identified for the as-deposited and annealed structures (Figs. 2(a) and 2(b)),

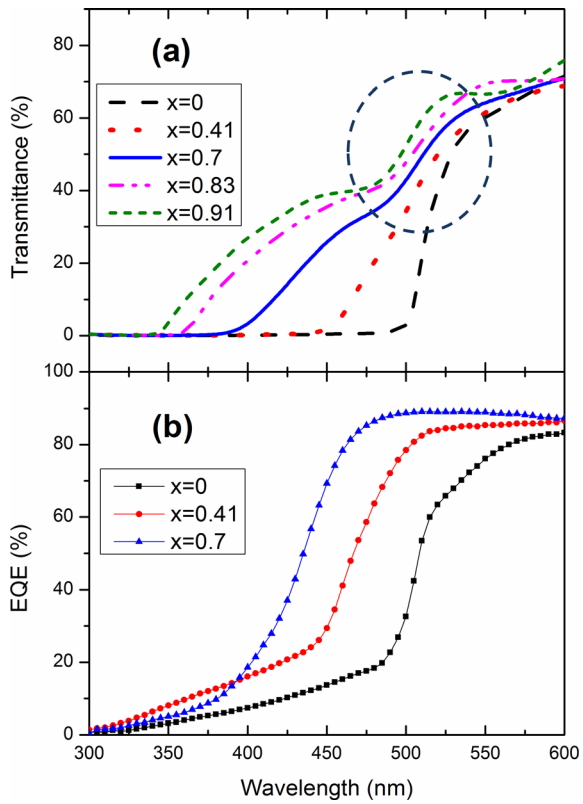

FIG. 1. (a) Transmittance spectra of $Cd_{1-x}Zn_xS$/CdS (450/50 nm) reference bi-layers deposited onto boro-aluminosilicate glass, and (b) EQE spectra of CdTe devices employing $Cd_{1-x}Zn_xS$/CdS (190/50 nm) bi-layers as the window layer. In (a) the contribution of the CdS film to the transmittance spectra is highlighted (dashed circle); this contribution is missing in the EQE spectra, indicating intermixing between the layers.

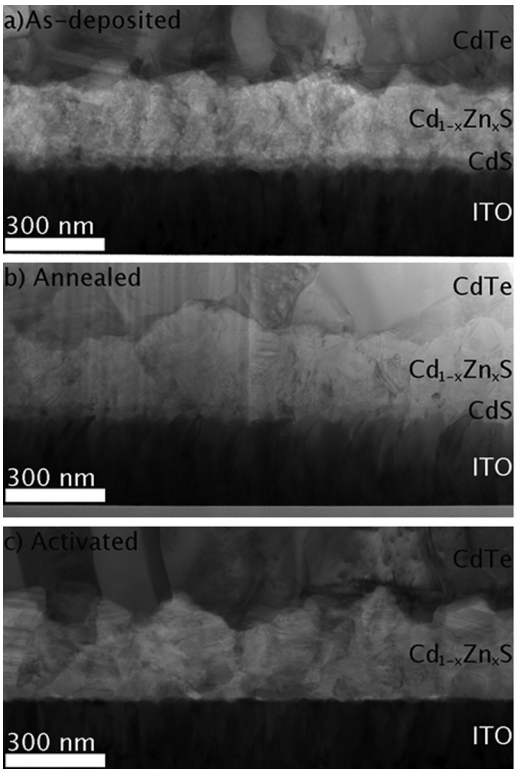

FIG. 2. Cross-sectional BFSTEM images of $CdTe/Cd_{1-x}Zn_xS/CdS/ITO/$ boro-aluminosilicate stacks around the window layer: (a) as-deposited, (b) annealed, and (c) $CdCl_2$ activated. Notice the loss of visibility for the CdS nucleation layer in (c).

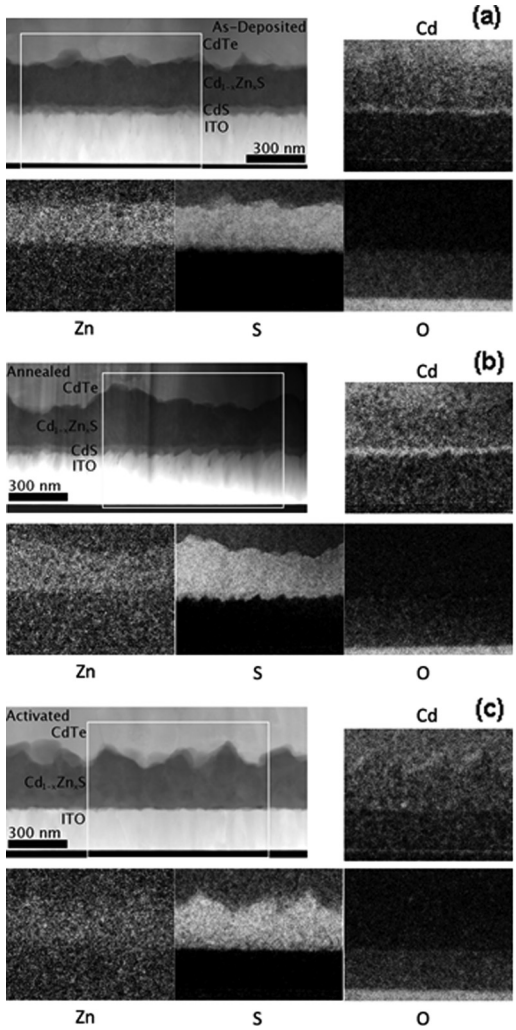

FIG. 3. HAADF STEM and EFTEM images (Cd, Zn, S, and O) of the $CdTe/Cd_{1-x}Zn_xS/CdS/ITO$ structures shown in Fig. 2: (a) as-deposited, (b) annealed, and (c) $CdCl_2$ activated. The white boxes in the HAADF STEM images indicate the region to which the EFTEM images correspond. Note the presence of a bright line in the Cd image at the $ITO/Cd_{1-x}Zn_xS$ interface for the as-deposited and annealed devices but not for the activated device.

this cannot be claimed for the activated device (Fig. 2(c)). The HAADF STEM images in Fig. 3 show a brighter layer at the window layer/TCO interface in the as-deposited and annealed devices, indicating higher average atomic number compared to the rest of the window layer. The EFTEM images in Fig. 3 have brighter contrast where the respective elements are located in the device; the bright line in the Cd-EFTEM images, for the as-deposited and annealed devices, demonstrates this layer to be Cd-rich compared to the rest of the window layer. The HAADF STEM and EFTEM data, therefore, qualitatively confirm the disappearance of the CdS layer and its merging into the $Cd_{1-x}Zn_xS$ layer via cation inter-diffusion. Hence, EFTEM data indicate that cation inter-diffusion requires both the thermal anneal and the presence of Cl species as the Cd-rich seed layer is clearly visible after the anneal but not after the full $CdCl_2$ activation.

The Cl^{35}, Cl^{37}, S^{36}, and Te^{120} isotope depth profiles obtained by SIMS for a number of activated device structures are shown in Fig. 4, with the Te and S signals serving as a reference to identify the position of the $CdTe/Cd_{1-x}Zn_xS$ interface. The minor isotopes of S and Te (mass 36 abundance 0.020% and mass 120 abundance 0.096%, respectively) were chosen to show the layer structure as their signal intensities were comparable with those from the Cl dopant. Unfortunately, there is an interference in the Te^{120} signal from Sn^{120} once the ITO layer is reached. The $CdTe/Cd_{1-x}Zn_xS$ interface is where the Te signal decreases and S signal significantly rises (at $\sim 2\,\mu m$); meanwhile the $Cd_{1-x}Zn_xS/ITO$ interface is where the Sn^{120} signal rises. The quantified Cl^{35} and Cl^{37} isotope traces, which have been corrected for their respective isotopic abundance, completely overlap in each sample shown. This indicates Cl signals are indeed due to Cl species and not related to other species with similar masses (e.g., $S^{34}H^1$, $S^{36}H^1$). It then becomes clear that Cl exists uniformly throughout CdTe and further into the $Cd_{1-x}Zn_xS$ window layer. However, the quantification of the Cl concentration ($atoms/cm^3$) within the $Cd_{1-x}Zn_xS$ layer could not be reliably obtained (due to the lack of an appropriate reference sample for this matrix) and hence the Cl concentration in Fig. 4 was obtained for the CdTe matrix using a CdTe film implanted with Cl as a reference sample. Nevertheless, there is sufficient evidence that Cl species diffuse down to the CdS/ITO interface, where they can catalyse the cation inter-diffusion behaviour; leading to $CdS–Cd_{1-x}Zn_xS$ intermixing.

Empirical evidence for the presence of Cl within the window layer can also be suggested from the observation that $CdCl_2$ activated and unactivated p-n junction structures clearly behave differently towards manual

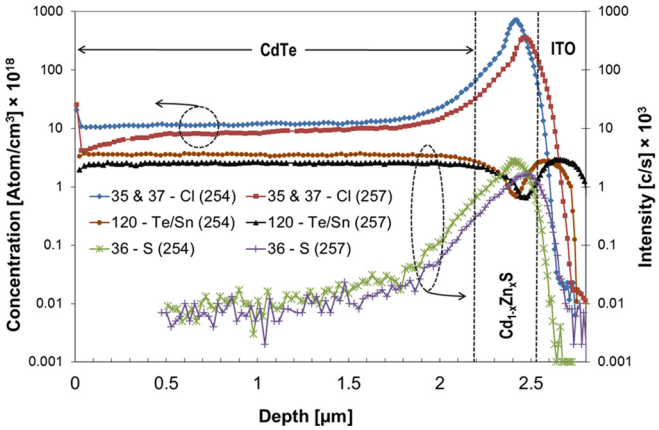

FIG. 4. Cl, S, and Te depth profiles for a number of $CdCl_2$ activated $CdTe/Cd_{1-x}Zn_xS/CdS/ITO/boro\text{-}aluminosilicate$ devices (254 and 257), confirming the presence of Cl species within the window layer. Te and S signals serve as reference for the $CdTe/Cd_{1-x}Zn_xS$ interface.

scraping (using a blade) of the coating from the ITO/glass surface. While in the former case the entire p-n junction could be removed with ease, the window layer in unactivated samples could not be removed by this process. Therefore, it appears that chemical transitions take place within the window layer upon $CdCl_2$ activation, causing some physical changes including the reduction of window layer adhesion to the substrate surface.

B. Structural changes in devices

Several other observations can be made from the STEM images of the three samples featured in Figs. 2 and 3. First, from the BFSTEM images, it could be seen that the window layer recrystallized and that the roughness of the $Cd_{1-x}Zn_xS/CdTe$ interface increased following both annealing and activation treatments. Both effects were observed to be greater after $CdCl_2$ activation. Others have also made this observation for CdS/CdTe cells,[15,16] though in those examples major restructuring was observed in both the CdS and CdTe layers. The results presented here demonstrate that while annealing produces similar effects to the full $CdCl_2$ activation, these effects are enhanced in the presence of Cl.

C. Chemical changes in devices

EDS line profiles obtained across the $Cd_{1-x}Zn_xS$ layer served to better compare the distribution of Zn and Cd in the three samples (Fig. 5). First, it is further confirmed that the thin layer (<50 nm) from the ITO surface in the as-deposited and annealed samples is almost pure CdS, which is lacking in the activated sample. Second, the Cd/Zn (at. %) ratio in the as-deposited sample varies from about 15/35 near the CdS layer to about 20/30 in the rest of the $Cd_{1-x}Zn_xS$ layer, corresponding, respectively, to $x = 0.7$ and 0.6, in close agreement to the nominal composition ($x = 0.7$) calculated for the corresponding reference layer by means of optical and X-ray detection methods.[2] From this, it can be suggested that first a Zn-rich layer nucleates on the CdS seed layer then followed by the growth of a fixed $Cd_{1-x}Zn_xS$ alloy composition, as the window layer structure was formed. After activation treatment, Zn diffusion into the CdS layer results in a Cd-rich $Cd_{1-x}Zn_xS$ composition, in the region of the seed layer. Furthermore, the composition is not totally homogeneous through the window layer, being more Zn-rich in the centre, and the Cd/Zn ratio has slightly changed in favour of Cd, providing further evidence for the cation inter-diffusion in the presence of Cl species. On the other hand, annealing appears to have led to some homogenisation of the $Cd_{1-x}Zn_xS$ layer. The ability of $CdCl_2$ activation to enhance inter-diffusion has previously been reported[16,17] but in the case of S (from the CdS window layer) into CdTe, it is interesting to observe here the inter-diffusion effects in $Cd_{1-x}Zn_xS$ alloy window layers.

The diffusion of S into CdTe (Fig. 6) is also affected by the annealing and activation treatments. Both annealing and activation somewhat enhance the extent to which S diffuses into CdTe. As with the window layer, the diffusion is more strongly affected by the Cl-activation than by the annealing alone. However, the relative change in the diffusion profile and diffusion depth between the three samples is less than that observed in the window layer and considerably less than that observed in previous studies.[16,17] This is consistent with the minimal structural changes observed in the CdTe following activation. This also further emphasises the important

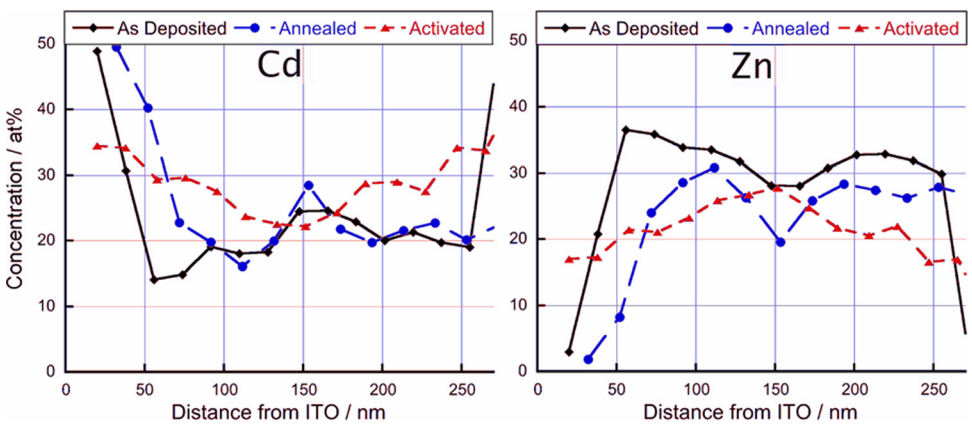

FIG. 5. EDS line scan data showing the changes in Cd and Zn depth profiles within the window layer for $CdTe/Cd_{1-x}Zn_xS/CdS/ITO$ baseline device stacks in response to post-deposition annealing and activation treatments. Trend lines are added to guide the eye.

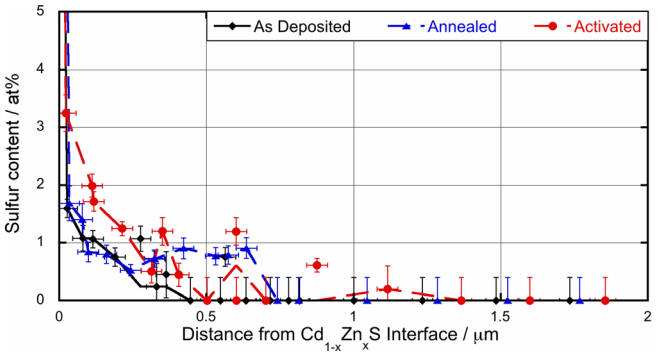

FIG. 6. Standardised EDS line scan data measuring the extent of S diffusion into the CdTe absorber for the as-deposited, annealed, and activated devices. The relative change in S diffusion for the different devices is significantly lower than the relative changes in Cd and Zn distribution in the window layer. Trend lines are added to guide the eye.

role that even a gentle (low temperature) Cl-activation can have on the $Cd_{1-x}Zn_xS$ alloy window layers investigated here.

IV. CONCLUSION

Chemical and structural changes in CdTe solar cells employing wide bandgap $Cd_{1-x}Zn_xS$ window layers have been studied in relation to post-deposition treatments using transmission electron microscopy and depth profiling methods. It is determined that recrystallization and inter-diffusion effects take place in the window layer and, to a lesser extent, in the CdTe. This results in interlayer mixing (with a CdS nucleation layer) as well as compositional variations of the $Cd_{1-x}Zn_xS$ layer, primarily due to $CdCl_2$ treatment. Of particular note is that the presence of Cl greatly enhances both window layer restructuring and cation inter-diffusion over the heat treatment alone. This leads to the necessity for tight control in the $CdCl_2$ treatment.

ACKNOWLEDGMENTS

The authors are grateful for funding from Engineering and Physical Sciences Research Council UK (EP/K008633/1, EP/I028781/1) and the European Regional Development Fund (SPARC project through the Low Carbon Research Institute).

[1]M. A. Green, K. Emery, Y. Hishikawa, W. Warta, and E. D. Dunlop, "Solar cell efficiency tables (version 41)," Prog. Photovoltaics: Res. Appl. **21**, 1–11 (2013).
[2]G. Kartopu, A. J. Clayton, W. S. M. Brooks, S. D. Hodgson, V. Barrioz, A. Maertens, D. A. Lamb, and S. J. C. Irvine, "Effect of window layer composition in $Cd_{1-x}Zn_xS$/CdTe solar cells," Prog. Photovoltaics: Res. Appl. **22**, 18–23 (2014).
[3]X. Wu, Y. Yan, R. G. Dhere, Y. Zhang, J. Zhou, C. Perkins, and B. To, "Nanostructured CdS:O film: Preparation, properties, and application," Phys. Status Solidi C **1**, 1062–1066 (2004).
[4]U. Jahn, T. Okamoto, A. Yamada, and M. Konagai, "Doping and intermixing in CdS/CdTe solar cells fabricated under different conditions," J. Appl. Phys. **90**, 2553–2558 (2001).
[5]K. Durose, P. R. Edwards, and D. P. Halliday, "Materials aspects of CdTe/CdS solar cells," J. Cryst. Growth **197**, 733–742 (1999), and references therein.
[6]M. A. Islam, M. S. Hossain, M. M. Aliyu, M. R. Karim, T. Razykov, K. Sopian, and N. Amin, "Effect of $CdCl_2$ treatment on structural and electronic property of CdTe thin films deposited by magnetron sputtering," Thin Solid Films **546**, 367–374 (2013).
[7]Y. Yan, R. G. Dhere, K. M. Jones, and M. M. Al-Jassim, "Influence of substrate structure on the growth of CdTe thin films," J. Appl. Phys. **89**, 5944–5949 (2001).
[8]M. Hädrich, N. Lorenz, H. Metzner, U. Reislöhner, S. Mack, M. Gossla, and W. Witthuhn, "CdTe–CdS solar cells–Production in a new baseline and investigation of material properties," Thin Solid Films **515**(15), 5804–5807 (2007).
[9]D. Grecu and A. D. Compaan, "Rutherford backscattering study of sputtered CdTe/CdS bilayers," J. Appl. Phys. **87**, 1722–1726 (2000), and references therein.
[10]A. J. Clayton, S. J. C. Irvine, E. W. Jones, G. Kartopu, V. Barrioz, and W. S. M. Brooks, "MOCVD of $Cd_{(1-x)}Zn_{(x)}S$/CdTe PV cells using an ultra-thin absorber layer," Sol. Energy Mater. Sol. Cells **101**, 68–72 (2012).
[11]J. Zhou, X. Wu, G. Teeter, B. To, Y. Yan, R. G. Dhere, and T. A. Gessert, "CBD-$Cd_{1-x}Zn_xS$ thin films and their application in CdTe solar cells," Phys. Status Solidi B **241**(3), 775–778 (2004).
[12]S. J. C. Irvine, V. Barrioz, D. Lamb, E. W. Jones, and R. L. Rowlands-Jones, "MOCVD of thin film photovoltaic solar cells—Next-generation production technology?," J. Cryst. Growth **310**, 5198–5203 (2008).
[13]A. A. Taylor, J. D. Major, G. Kartopu, D. A. Lamb, V. Barrioz, A. J. Clayton, J. Duenow, R. Dhere, H. Moutinho, S. J. C. Irvine, K. Durose, and B. G. Mendis, "A comparative STEM study of sulfur diffusion in CdS/CdTe thin film photovoltaics" (unpublished).
[14]L. A. Giannuzzi and F. A. Stevie, "Focused ion beam milling for TEM specimen preparation," Micron **30**, 197–204 (1999).
[15]B. E. McCandless, L. V. Moulton, and R. W. Birkmire, "Recrystallization and sulfur diffusion in $CdCl_2$-treated CdTe/CdS thin films," Prog. Photovoltaics: Res. Appl. **5**, 249–260 (1997).
[16]M. Terheggen, H. Heinrich, G. Kostorz, D. Baetzner, A. Romeo, and A. N. Tiwari, "Analysis of bulk and interface phenomena in CdTe/CdS thin-film solar cells," Interface Sci. **12**, 259–266 (2004).
[17]W. K. Metzger, D. Albin, M. J. Romero, P. Dippo, and M. Young, "$CdCl_2$ treatment, S diffusion, and recombination in polycrystalline CdTe," J. Appl. Phys. **99**, 103703–103708 (2006).